

(X)MET: DESIGN AND TEST OF MICROWAVE ELECTROTHERMAL THRUSTERS WITH ARGON AND XENON

SPACE PROPULSION 2020+1

17 – 18 – 19 MARCH 2021

D. Staab⁽¹⁾, S. Reeve⁽¹⁾, T. Baxter⁽²⁾, E. Lekuona⁽¹⁾, H. Larsen⁽¹⁾, E. Longhi⁽¹⁾, K. Swar⁽¹⁾, A. Garbayo⁽¹⁾, C. Ryan⁽²⁾

⁽¹⁾ AVS UK Ltd - Rutherford Appleton Laboratory, Chilton, (United Kingdom), Email: dstaab@a-v-s.uk.com

⁽²⁾ University of Southampton, Southampton (United Kingdom)

KEYWORDS: electrothermal thrusters, electric propulsion, microwave, xenon, all-electric

ABSTRACT:

This work presents design upgrades and test results of XMET, a Xenon Microwave Electro-thermal Thruster. XMET uses a free-floating plasma discharge in a cylindrical resonant cavity operating at 2.45 GHz. It will be used as the reaction control system thruster for an integrated propulsion architecture for small GEO platforms in combination with a microwave based gridded ion engine. We discuss the theoretical background of METs, previous work and describe prototype optimisation done for XMET. Results from an extended test campaign characterising several breadboard configurations are given.

1. Introduction

1.1. All electric IMPULSE architecture

The Integrated Microwave Propulsion Architecture for Telecommunication Satellites (IMPULSE) is a highly innovative propulsion architecture for small all-electric geostationary (GEO) platforms. Development has been funded by the UK Space Agency's National Space Technology Programme (NSTP), and is a collaboration between the University of Southampton, AVS UK and the STFC-ISIS group.

IMPULSE will enable GEO spacecraft with fully all-electric propulsion for station keeping, orbit raising, and attitude control. "Fully all-electric" here refers to the concept of a highly integrated primary and secondary propulsion system [1]. This reduces propulsion system mass, cost and complexity and completely eliminates the use of hydrazine, a key operational and safety benefit. IMPULSE uses X-EPT, a Gridded Ion Engine (GIE) and Neutraliser, both exploiting microwave-based electron cyclotron resonance (ECR) for primary propulsion, combined with microwave electro-thermal thrusters (MET) in the auxiliary propulsion system. The same Xenon

propellant tank feeds all systems; therefore we refer to our RCS thruster as XMET. X-EPT and XMET are powered a common solid state microwave generator at 2.45 GHz. The system level electrical architecture is simplified compared to conventional GIEs: separate discharge cathode heater & keeper, neutralizer heater & keeper, anode and solenoid supplies are no longer required. The microwave generator common to XMET, X-EPT is combined with a single high voltage accelerator supply, significantly reducing system complexity.

Initial development and testing of the first prototype X-EPT and XMET devices have been previously reported [2],[3],[4]. A second-generation design of X-EPT is described in the companion paper [5] at SPC2020+1. The current paper will discuss the design and test of two new XMET prototype thrusters.

1.2. Core MET design principles

The fundamental operating principle of METs is the use of microwave (MW) energy to create a free-floating plasma discharge in a cylindrical cavity resonator, which efficiently heats gaseous propellants that are subsequently expanded through a conventional gas dynamic nozzle.

Microwave Electrothermal Thrusters follow the basic constraints from cylindrical resonant cavity theory. Establishing a useful plasma discharge with efficient heating of the propellant requires a resonant cavity mode in which the electric field strength peaks at the nozzle throat. As a result, the TM_{011} mode is used almost exclusively by METs, following [6]. With the mode fixed to TM_{011} , there remain two different design philosophies. The first is an axially symmetric electric field strength distribution, where the field peaks at either end of the cavity (at the nozzle inlet and antenna). The antenna is protected from plasma discharge via a dielectric plate at the cavity mid-plane, with a permittivity and thickness tuned to the cavity height and radius to maintain resonance. The alternative

is a concept demonstrated by [7], in which the field is axially asymmetric, and the dielectric disk is positioned at the antenna end of the cavity. This results in higher electric field strength at the nozzle throat, and thus may in principle provide greater heating capability and higher performance. This is at the expense of a sharper resonance than the symmetric cavity geometry (all else being equal), which in practice makes cavity tuning more challenging.

The propellant inlets follow the extensively proven vortex flow injection strategy [8] to stabilize the free-floating plasma discharge at the nozzle inlet. This is a pair of tangentially mounted inlets mounted to opposite sides of the cavity cylinder sidewall. The propellant is expanded through a conventional gas dynamic nozzle.

To optimise a given cavity design, the frequency and sharpness (FWHM) of its resonance are the key metrics and a balance must be struck between maximising the electric field strength at the nozzle throat while avoiding an overly small FWHM. Experimental optimisation of METs is required to reach the highest gas temperatures and thruster performance with good MW coupling (low reflected power). The influence of parameters such as the dielectric position, antenna size, throat and injector geometry should be investigated primarily.

1.3. Historical MET development

METs have been developed in the US over many decades, primarily at Penn State university using frequencies of 2.45 - 17.8 GHz, power levels of ~ 20 - 2000 W, and thrust levels of ~ 1 - 300 mN [8], [9]. There is renewed interest in METs for New Space applications as they are inexpensive, highly scalable, and compatible with a wide range of alternative propellants. Work has focussed on small satellite propulsion applications by using higher frequency, smaller resonant cavity designs, which leads to lower power but lower thrust devices. METs intrinsically have higher thrust to power ratio than more conventional electric propulsion solutions like GIEs, hall effect thrusters or FEEPs, and are at an advantage for mission applications where maximising specific impulse (ISP) is secondary compared to e.g. transfer orbit duration. METs compete with resistojets and arcjets at comparable thrust to power ratios but should be able to reach higher specific impulse (ISP) since the latter technologies are limited by thermal endurance of the resistive heating element and cathode erosion, respectively.

The free-floating plasma discharge inside the resonant cavity minimizes erosion of crucial components while no cathodes are required for either plasma generation or exhaust neutralization. METs have recently found commercial application with water propulsion for the orbital transfer

vehicles (tugs) of Momentus Space. The first on-orbit demonstration of a full propulsion module onboard a cubesat has been successfully completed [10].

A MET developed at Bogazici University Space Technologies Laboratory (BUSTLab) is the only optimised 2.45 GHz, 200 W class prototype that has been developed to our knowledge, reaching up to 100 s ISP and thruster efficiency η_t of 40-60% with Argon from direct thrust measurements [11]. Due to propellant cost, the vast majority of our testing is also carried out with Argon, therefore the BUSTLab thruster is our main reference benchmark.

The IMPULSE architecture limits the achievable XMET specific impulse compared to propellants with much lower molecular weight than Xenon and increases the achievable thrust to power ratio (TTPR). We are not aware of any Xenon MET results in the literature to date. Conventional Xenon resistojets such as the SSTL T-30 are restricted to chamber temperatures T_c below 1000 K by material (erosion) limits, resulting in a practically achievable ISP ceiling of ~50 s with Xenon [12]. For reference, the highest chamber temperatures achieved in the MET literature, to date at the ~1kW power level using nitrogen propellant was ~3500 K [8]. A comparison of resistojet, the most recent 2.45 GHz BUSTLab data published and our performance goals for XMET in the IMPULSE project is given in Tab.1. Argon performance goals have been derived from the Xenon case by assuming identical chamber temperature can be reached, i.e. scaling the ISP by the square root of the specific heats, 158 J kg⁻¹K⁻¹ and 520 J kg⁻¹K⁻¹ respectively.

Table 1: Comparison of our XMET performance goals with an operational resistojet and relevant MET data from literature.

thruster	prop	thrust [mN]	ISP [s]	T_c [K]	η_t [%]	TTPR [mN/W]	power [W]
SSTL T-30 [12]	Xe	~100	48	~750	78	3.3	30
MET BUST Lab [11]	Ar	~200 - 300	80-100	600-920	40-60	0.9 - 1.4	200
XMET	Ar	150	135	1700	50	0.75	200
XMET	Xe	300	75	1700	55	1.5	200

1.4. First generation XMET

The IMPULSE-I XMET design is fully described in [2],[3]. It utilized the asymmetric electric field concept, referred to hereafter as the bottom plane design. An adjustable cavity length was implemented via a threaded interface between two halves of the cavity, to give manual control over its resonant frequency while using a fixed 2.45 GHz

MW generator. Early testing demonstrated low power ignition matching the expected microwave plasma breakdown behavior of Argon. A small subset of tests showed good performance with thrust reaching 140 mN and specific impulse ~ 110 s at flow rates < 125 mg/s and 200 - 400 W forward power from the generator. Subsequent campaigns were unable to repeat these results, with poor coupling of the microwave power to the propellant. Visual inspection suggested the plasma was forming lower in the cavity than expected, and thus not effectively heating the propellant at the nozzle. Cold flow results showed good agreement with isentropic flow theory, and Vector Network Analyser (VNA) measurements showed the cavity was well matched to the 2.45 GHz frequency, within the adjustable height range,

1.5. Isentropic Flow Theory and Discharge Coefficient

Thruster characterisation is carried out using an indirect thrust measurement approach, this allows for quick iteration of the flexible breadboard while giving a good indication of performance and clear relative performance between configurations. Direct thrust measurement and performance validation using a thrust balance is left for future work once the thruster configuration is optimised.

As with any other type of gas dynamic nozzle, the standard isentropic flow relations provide a good basis for this. Monatomic single species propellants of Xenon and Argon, where γ and R are well known, are particularly suitable to this approach. The assumption can be made that the flow at the nozzle throat will always be choked, as such the Mach number at the exit plane of the nozzle is dependent only upon the expansion ratio. Negating the pressure term, thrust is simply defined as the mass flow rate multiplied by the exit velocity. The mass flow rate is known while the exit velocity can be calculated based on the exit Mach number and local speed of sound, Eq. 1.

$$V_{ex} = Ma = M\sqrt{\gamma RT} \quad \text{Eq. 1}$$

This requires knowledge of the local gas temperature at the nozzle exit. This can be derived from the Isentropic flow relations, Eq. 2.

$$\frac{T}{T_0} = \left(1 + \frac{\gamma - 1}{2} M^2\right)^{-1} \quad \text{Eq. 2}$$

Where T is the local gas temperature and T_0 is the chamber stagnation temperature. For an ideal gas at constant volume, the ratio of temperatures and pressures can be related to one another using:

$$\frac{T_h}{T_c} = \left(\frac{P_h}{P_c}\right)^{\frac{\gamma-1}{\gamma}} \quad \text{Eq. 3}$$

Where T_h is the stagnation temperature while operating with microwave power and T_c is the temperature at the same flow rate with no microwave power, respectively referred to as "hot flow" and "cold flow". The remaining unknown therefore is the chamber pressure, easily measured experimentally using a simple transducer and pressure tapping. T_c is known, 295 K, while P_c can be experimentally measured for a range of flow rates, during a "cold flow" sweep. Therefore T_c can be related to the measured quantity P_c while operating in "hot flow".

While this approach provides a good indication of thruster performance, it does not account for some of the additional losses that are incurred for nozzles with small throat area. For large throat area thrusters, the isentropic flow relations are satisfactory as the boundary layer thickness is negligible compared against the throat diameter. As thruster size decreases, the thickness of the boundary layer grows as a relative proportion of the throat diameter, manifesting as an effective reduction in the nozzle throat area and increasing chamber pressure. This behaviour can be seen in the cold flow data presented in section 4.2.

In order to account for this loss the Isentropic flow equations can be modified with the inclusion of a discharge coefficient, C_d , term. This is simply the ratio between the actual mass flow throughput and the theoretical isentropic mass flow (Eq. 4).

$$C_d = \frac{\dot{m}_{actual}}{\frac{A^* P_c \sqrt{\gamma}}{\sqrt{RT_c}} \left(\frac{2}{\gamma + 1}\right)^{\frac{(\gamma+1)}{2(\gamma-1)}}} \quad \text{Eq. 4}$$

The Discharge coefficient varies with mass flow rate, nozzle geometry, and gas temperature. As such a constant coefficient cannot be applied to each nozzle. The Reynolds number R_e is the fundamental property driving the boundary layer thickness as defined by Eq. 4.

$$R_e = \frac{\rho^* u^* d^*}{\mu^*} = \frac{\dot{m}}{\frac{1}{4} \pi d^* \mu^*} \quad \text{Eq. 5}$$

Where d^* is the geometric throat area and μ^* is the kinematic viscosity, a function of temperature given by Eq. 6 for Argon.

$$\mu(T) = 4.92 \times 10^{-8} T + 8.465 \times 10^{-6} \quad \text{Eq. 6}$$

Using the cold flow data obtained at $T \sim 295$ K, Eq. 4 and Eq. 5 define a relation between Reynolds Number and Discharge Coefficient (Fig. 1). Substituting Eq. 6 into Eq. 5, rearranging for temperature and substituting into Eq. 4 produces a second function relating Reynolds Number to Discharge Coefficient.

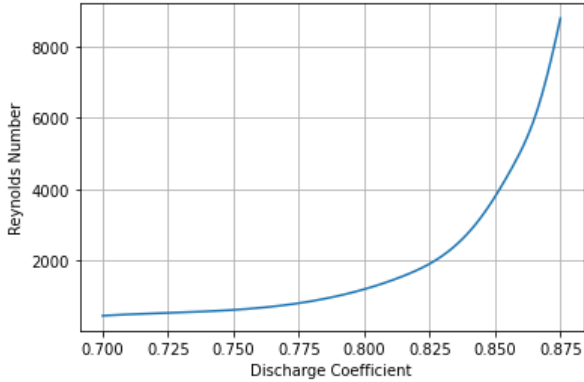


Figure 1. An example of the relationship between Reynolds Number and Discharge Coefficient, derived from cold flow measurements.

These functions are solved simultaneously to derive the Discharge Coefficient, with Eq. 4 then being used to calculate the Boundary layer compensated isentropic chamber temperature. This is the approach used in our data analysis. All other thruster key performance metrics (thrust, vacuum ISP, efficiency) can be indirectly derived from this compensated chamber temperature combined with Eq. 1, measurement of the power delivered to the thruster and the known nozzle area ratio (200 for XMET), under the assumption of perfectly expanded exhaust and negligible cosine losses (< 2%) for our simple conical geometries with half angle 15 deg.

2. XMET second generation design

2.1. Changes relative to IMPULSE-I

After the first generation test campaign, the fixed frequency 2.45 GHz MW generator was replaced by a solid state generator with precisely selectable frequency over 2.4 - 2.5 GHz with 1 MHz resolution, and in-built forward & reflected power measurement. Combined with stub tuning capability on the MW feedline, this ensures the cavity remains on resonance with a good impedance match, without the need for the geometry adjustment of the first generation.

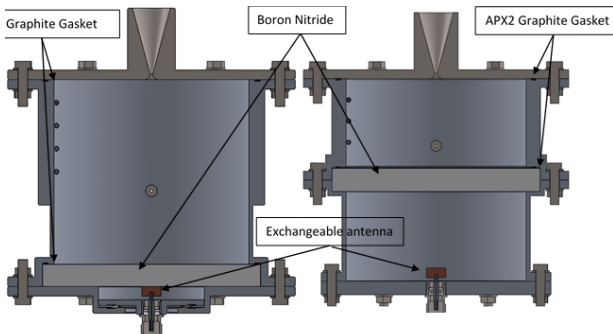


Figure 2. Cross-sectional view of bottom plane (left) and mid plane (right) dielectric variants of the 2nd generation XMET.

A broad resonance relative to the 1 MHz step size of the generator is required to ensure the peak electric field strength is achieved. The 1st generation XMET was optimised towards the highest possible field strength with an extremely sharp resonance, which was likely part of the difficulty encountered in stable, repeatable operation. In IMPULSE-II, we therefore targeted broader resonances of ~10 MHz or higher, accepting a reduction in maximum field strength. Our approach was to build two new thruster variants (Fig. 2); one a bottom plane cavity with broadened resonance compared to the first generation, and a second with symmetric resonance, the dielectric in the mid plane of the cavity, matching the much more extensively tested MET designs in literature. For the latter, a significantly lower field strength but broader resonance is inherent.

For both thrusters, a set of exchangeable copper antennas of different sizes were baselined. These interface with the 7/16 coaxial connector feed from the microwave line and couple the input power to the cavity. As in [8], multiphysics modelling was used to size the two cavities, dielectrics, and the antenna sizes, targeting a range of combinations of resonance FWHM and maximum electric field strength at the nozzle inlet, E_{max} (Fig.3, Fig.4). This allows experimental testing of which resonant configuration maximises thruster performance.

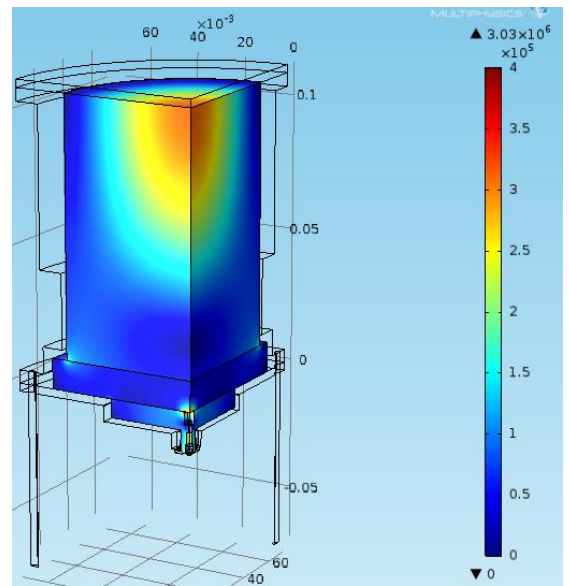


Figure 3. Quarter-section view of modelled field strength (V/m) within the cavity of a bottom plane XMET configuration at 400 Watts input power; pre-ignition. The field strength is maximised at the nozzle inlet location.

A key visual observation during IMPULSE-I testing was the plasma discharge location, extending further away from the nozzle inlet than expected. This may have prevented it from acting as the stable nozzle inlet plug required for effective propellant heating, causing poor performance.

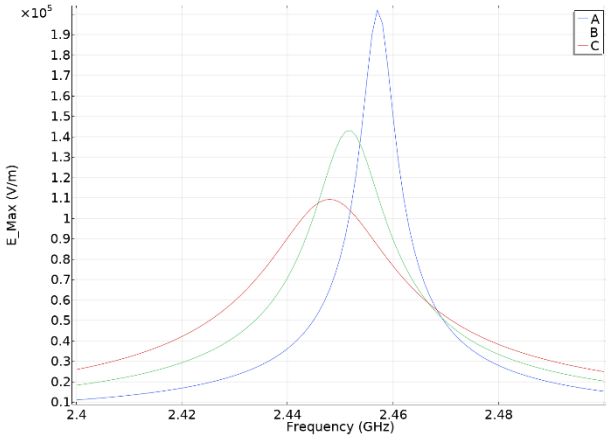


Figure 4. Modelled field strength at nozzle inlet for the mid plane XMET, with the set of 3 antenna sizes increasing from A-C.

Such behaviour can be connected to a non-ideal vortex flow pattern, as this interacts with the electric field to fix the exact discharge location and shape. We therefore required the injector positions and diameters to be adjustable in the 2nd generation thrusters. In summary, the main changes are:

- Mass reduction & Fixed cavity geometry.
- Flexible injector position, diameter, and antenna.
- Broader resonance response.
- Boron Nitride grade change from X05 to M26

2.2. Materials and Interfaces

The XMET thrusters consist of either one (bottom plane) or two (mid plane) cylindrical chambers, to which the baseplate assembly (7/16 connector & antenna) and exchangeable nozzle plate are mounted. The Boron Nitride disk is housed either between the two chambers (mid plane) or between the chamber and baseplate (bottom plane). The cavity is sealed against internal pressure with graphite gaskets. The cavity wall accommodates the pressure transducer line, observation window and exchangeable injector interface (Fig. 5).

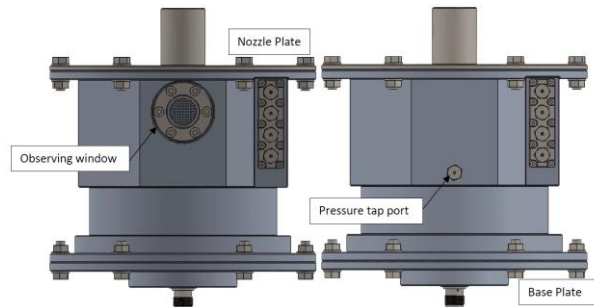


Figure 5. Bottom plane XMET external interfaces.

The sapphire observing window is obstructed by a grid machined into the cavity wall, avoiding MW leakage and modification of resonance properties. Aluminium 6061-T6 is used for the thruster chamber and base plate. The nozzle plate material

is SS 316L, maintaining a higher temperature compatibility. The overall weight is reduced to ~2.3 kg compared to the ~ 5 kg 1st generation XMET. Note the 2nd generation XMET's are still laboratory breadboards designed for flexibility and are far from flight-like mass optimization. For a flight unit much lower mass can be reached even for an all-steel thruster, via changes such as removing the viewport and the assembly that allows multiple injector configurations, combined with additive manufacturing to minimize chamber wall thickness.

3. Test Campaign

3.1. Experimental Setup

Testing is conducted in the David Fearn Electric Propulsion Laboratory at the University of Southampton (Fig. [Error! Reference source not found.6](#)). A Leybold LeyVac LV140C pump provides rough pumping capability, backing up two Leybold TURBOVAC MAG W2200iP turbomolecular pumps. Two further compressor units (Coolpack 6000H) with two cold heads (Coolpower 140T) are attached to the test chamber. An ultimate base pressure of <1.0E-7 mbar is reached with operation <1E-4 mbar at ~150 mg/s Argon flow rate. Chamber pressure is monitored by a Pfeiffer Vacuum PKR 251 Gauge with a Pirani sensor and an inverted magnetron cold cathode gauge.



Figure 6. Mid-plane XMET with coaxial line, propellant feed and pressure tap lines attached, mounted in the vacuum chamber for testing.

For normal operation of XMET, the thruster was connected to a solid-state Kuhne SG 2.45-250A variable frequency microwave power supply via a triple-stub tuner. The microwave line including all cabling, vacuum feedthroughs, tuners, and adaptors, resulted in an overall insertion loss of 0.79 dB (17%). This was measured using a microwave power meter in place of the thruster, with the triple stub tuners set at the nominal zero protrusion. Forward and reflected power levels, P_F

and P_R , are measured at the generator throughout the test campaign, a simple calculation using this measured insertion loss (IL) gives the actual power delivered to the thruster, P_D (Eq.7).

$$P_D[W] = P_F[W](1 - IL) - \frac{P_R[W]}{(1 - IL)} \quad \text{Eq. 7}$$

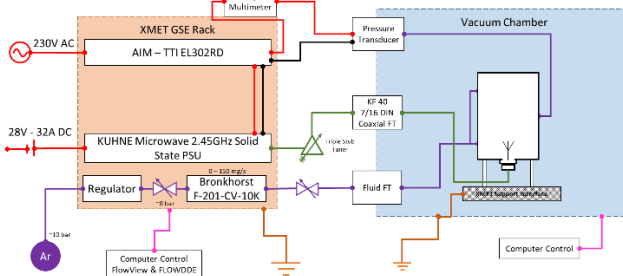


Figure 7. XMET test setup.

Propellant was controlled by a Bronkhorst F-201-CV-10K mass flow controller with regulated 4 bar supply pressure. Thruster pressure measurements were taken by an absolute pressure transducer, connected via vacuum feedthrough to a pressure tapping port on the thruster. For configuration changes affecting the resonance response (antenna or dielectric position), the resonant frequency and S11 response was measured using a VNA. This was done without the stub tuner attached, to remove any impedance change it imparted on the thruster. The VNA data defined the best frequency of operation for each configuration, and verified the computational analysis conducted in the design phase.

3.2. Operating Approach

Argon was used for all characterisation tests, with a goal of identifying the best performing thruster configuration and trends in the parameter space, before moving to the expensive Xenon propellant. Before each configuration was tested, cold flow data was taken up to the maximum hot flow data point, cold flow data at flow rates lower than expected operating values is important to ensure the relation in Fig. 1 is well defined. The resulting chamber pressure was compared to isentropic predictions, for leak detection and to characterise the nozzle discharge coefficient. The accuracy of cold flow data is crucial for the pressure ratio based performance characterisation, therefore the process was repeated after hot-fire, to ensure no erosion of the nozzle or other damage had occurred that could bias the pressure ratio data. Numerical analysis predicted that approximately 30-50 W of delivered microwave power would be required for plasma breakdown to occur at the lowest chamber pressure achievable with the test setup. Using the lowest Argon flow rate possible from the mass flow controller (3 mg/s) at the resonant frequency identified via the VNA typically allowed repeatable ignition at 50 W. In some cases

a sweep of stub tuner positions was required to find a good impedance match with the cavity, i.e. minimise reflected power pre-ignition.

The presence of a plasma naturally changes the impedance of the resonant cavity following ignition. This required re-adjusting the triple stub tuner to again find an optimal tuning with minimised reflected power when ignited. As the mass flow rate was increased from ~3 mg/s to ~30 mg/s, the plasma density and distribution in the resonant cavity changed significantly, and the cavity impedance tuning was adjusted accordingly. Above 50 mg/s, optimal tuning did not require significant further adjustment.

Once ignited, operation of XMET is relatively simple: MW forward power at the generator can be increased to the desired set-point level followed by a sweep of flow rates, taking stable chamber pressure readings at each desired flow rate. This approach yielded highly repeatable results. Plasma instability and resulting rapid increase in reflected power sporadically caused self-extinguishing behaviour while sweeping through flow rates. In these cases, a strategy of first setting the desired flow rate at a lower power level and then increasing power to the desired setpoint was used successfully. The same set of 6 forward power levels covering the 50 - 250 W range were used throughout the test campaign. Coupling efficiency was consistently maintained at > 95 %. The power delivered to the thruster was therefore between 40 - 210 W, as governed by the line insertion loss.

4. RESULTS

4.1. VNA Results

VNA measurements show good agreement with the computational analysis (Fig. 8). The selected M26 grade of Boron Nitride has a non-isotropic Dielectric Constant and loss tangent, dependant on the orientation of the grain structure. Combined with manufacturing tolerances, this is believed to be the primary driver of the ~20 MHz discrepancy between simulation and measurement.

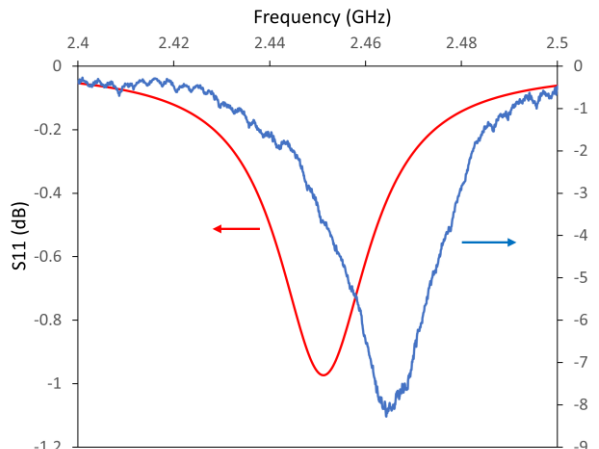


Figure 8. Comparison between simulation (red) and VNA measurement (blue) of the cavity frequency response.

4.2. Cold Flow Results

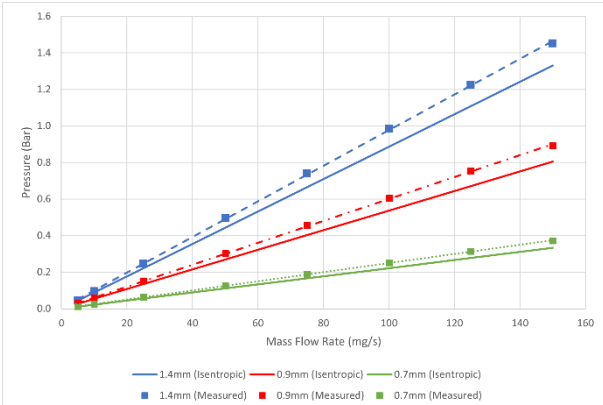


Figure 9. Cold flow chamber pressure measured for 3 nozzle throat diameters (dashed linear fits) compared to isentropic predictions with discharge coefficient of 1.

Cold flow data was highly repeatable for a given nozzle size across the campaign. As seen in Fig.9, the cold flow chamber pressures were consistently higher than predicted from isentropic flow theory, as expected for a discharge coefficient below 1. Cold flow testing ruled out any significant leaks in the propellant feed lines or thruster, and showed the repeatable behaviour required for accurate pressure ratio performance characterisation. Over the mass flow rates of interest for hot fire above 50 mg/s, this data is consistent with cold flow discharge coefficients ranging 0.84-0.89 for all nozzles.

4.3. Plasma Behaviour

XMET showed a distinct set of plasma regimes during operation, each with varying performance characteristics. A diffuse plasma regime was seen upon ignition, and at very low flow rates. The plasma appeared to be uniformly distributed over the visible volume of the resonant cavity.

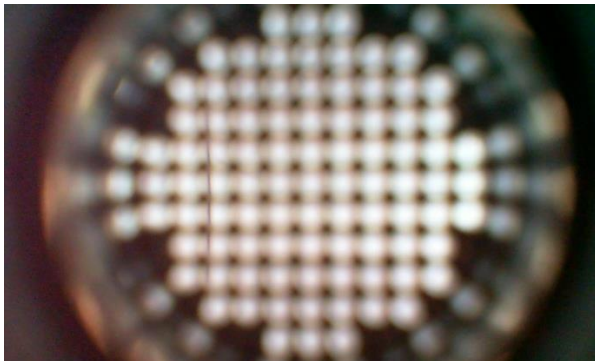


Figure 10. Diffuse Plasma Regime viewed through the cavity window.

When increasing flow rate, a gradual transition would occur, whereby the plasma would coalesce below the nozzle throat. The plasma appeared to flicker, changing shape in the radial direction. This regime resulted in the best thruster performance (highest cavity pressures at a given set-point) but

did result in pressure fluctuations of around 2% in the mid-plane configuration, and <0.5% in the bottom-plane configuration. The glowing plasma volume increased in size and brightness as the flow rate was increased.

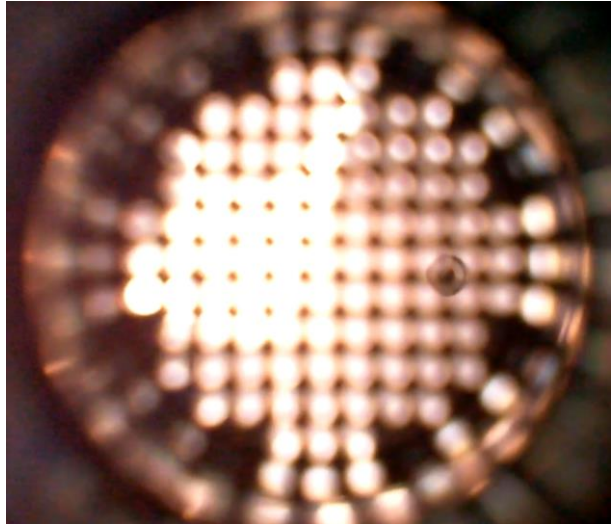


Figure 11. Viewport view of the best performing plasma regime. Nozzle inlet is on the left hand side.

At the higher flow rates tested, depending on which thruster configuration was tested, the plasma transitioned to a thin column-like regime along the central axis of the thruster chamber. The discharge shape was largely unchanged by flow rate and power input, however its brightness did vary with power. The latter two modes required very similar stub tuner positions to minimise reflected power, i.e. presented very similar impedance.

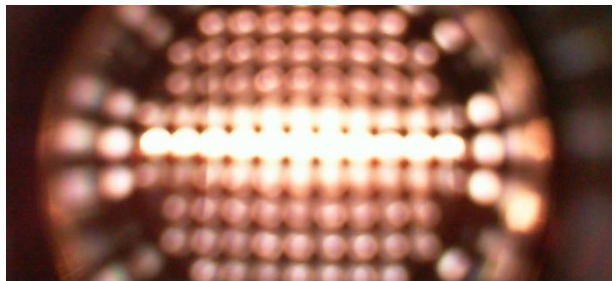


Figure 12. Viewport view of the column plasma regime. Nozzle inlet is on the left hand side.

When operating the thruster under only vacuum roughing pumps with a background pressure of ~50 Pa, clear flow separation of the plasma plume occurred (Fig.13), as expected for nozzle exit pressures of < 3 Pa. When firing XMET with turbopumps and cryopanels running, at background pressure of <0.01 Pa, the plasma plume appears almost perfectly expanded.



Figure 13. XMET plasma plume exiting the nozzle under rough (left) and high vacuum (right).

4.4. Hot fire pressure ratio based performance

We applied the procedure described in Section 1.5 using the cold flow data to correct hot fire chamber temperature values, by compensating for the boundary layer behaviour. The result was a chamber temperature up to 10% lower than the idealised isentropic assumption, with hot fire discharge coefficients ranging between 0.80 – 0.89 depending on nozzle geometry, flow rate and temperature.

We verified using repeated measurements at the same mass flow and input power for a given thruster configuration that (average) hot fire pressure readings were highly repeatable at the 5% level or better.

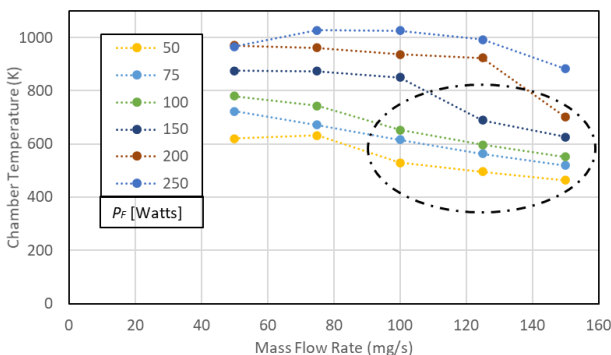


Figure 14. Complete T_c dataset measured for one XMET configuration. Transition to the column plasma regime occurred for the points circled. Dashed lines connecting common forward power levels are shown purely as visual aid.

As illustrated in Fig.14, chamber temperature trends followed consistent patterns over mass flow and input power: at lower P_f set-points, T_c decreased monotonically with \dot{m} while at high P_f ,

T_c peaked at intermediate \dot{m} as expected [8]. Similar lower power level T_c peaks should occur at lower flow rates than we tested but are less relevant to our test campaign due to insufficient thrust relative to the XMET target. The same patterns occurred across all configurations tested except one, where negligible propellant heating was observed at all set-points.

Data collection to date has focussed on the mid plane variant, testing all nozzle and antenna sizes combined with 2 injector positions. The smallest injector diameter was used for all but one configuration. Performance changes between configurations typically occurred as relatively consistent shifts across most of the P_f versus \dot{m} phase space. The T_c peak locations and trends with flow rate (i.e. chamber pressure) also varied. We observed that the transition between the plasma regimes of Fig. 11 and 12 (as \dot{m} was increased at a given P_f) corresponds to a prominent step change to lower T_c values, i.e. less effective heating. Note that given XMET's high thrust targets, the main performance levels of interest are those for the highest power and flow values.

Over the subset of configurations tested so far performance shifts between nozzle sizes (holding all other parameters constant), were of order 6-11 seconds of ISP, while changing injector position (all else being equal) drove ISP changes of 5-7 s.

4.5. Best performing XMET configuration

The mid-plane configuration using the smallest nozzle size and largest antenna was able to maintain high chamber temperature approaching 1000 K up to the highest flowrate tested (150 mg/s) at 250W forward power, resulting in the highest implied argon thrust throughout the campaign to date of 148 mN (Tab.2). Hot fire chamber pressure ranged from 0.99 - 2.74 bar. Our thrust target (Tab.1) was therefore achieved, but at significantly lower chamber temperature and ISP than aimed for.

The best performing configuration overall was the mid-plane, medium nozzle and largest antenna size variant, reaching our highest recorded T_c = 1027 K at 0.9 bar. Within the high thrust regime of primary interest for IMPULSE of > 120 mN, the highest efficiencies and TTPR achieved were $\sim 35\%$ and 0.7-1.0 mN/W. Further improvements in chamber temperature and ISP may be achieved in additional configuration tests, in the context of the trends described in Section 4.4.

4.6. Xenon data

At the time of writing, only partial performance data with Xenon for the latter configuration were obtained: a single forward power level of 150 W and flow rates of 165–415 mg/s. No boundary layer compensation has been applied to this data. High chamber temperature of 960 K (ISP = 56 s)

was maintained only at the lowest flow rate tested. At this 125W delivered power level, for flow rates ≥ 250 mg/s, T_c dropped below 650 K, which is roughly in-line with the behaviour of the uncompensated argon T_c data for this XMET configuration at equivalent power, volumetric flow range and chamber pressure. This low specific power regime tested to date limited the implied thrust range achieved with Xenon to 90-170 mN with thruster efficiency 20-28% and TTPR 0.7-1.4 mN/W. Xenon data collection above 150W forward power is ongoing and required before conclusions can be drawn on XMET performance with this propellant.

Table 2: 2nd generation XMET prototype results with argon propellant for two highest performing configurations at highest power level tested; 50-150 mg/s flow rate.

configuration	P_F [W]	P_o [W]	thrust [mN]	ISP [s]	η_t [%]	TTPR [mN/W]	T_c [K]
Mid-plane, 0.7 mm Nozzle	250	207-208	50-148	100-102	12-35	0.24-0.71	938-977
Mid-plane, 0.9 mm Nozzle	250	208-209	50-143	97-105	12-33	0.24-0.68	883-1027

5. CONCLUSION

Testing of the 2nd generation XMET thrusters validated their resonant cavity responses compared to predictions from modelling with an offset that can be attributed to uncertainty in the permittivity of the selected Boron Nitride grade. The XMETs prototypes were easily ignited and we successfully carried out steady state firing tests across our selected flow rate and input power set-points. Pressure ratio data were obtained from readings during hot fire and cold flow for extensive characterisation of the modular thruster prototypes and converted to boundary layer compensated chamber temperatures, ISP and thrust values. Testing showed highly repeatable pressure ratio based performance data for each thruster configuration, following consistent trends over mass flow and input power. This has allowed accurate relative performance characterisation between configurations, using Argon propellant. To date we have primarily obtained data for the mid plane variant. The full performance envelope of XMET will be explored in continued tests and direct thrust data will be acquired with Argon and Xenon to verify performance at further optimised parameters settings.

6. Acknowledgements

The IMPULSE-II project is supported and funded by the UK Space Agency as part of the National Space Technology Program (NSTP3-FT2-059). The authors would like to express their gratitude to the late Dr Angelo Grubišić for his key role in initiating the IMPULSE project.

7. REFERENCES

1. Wells, N., Walker R., Green S. and Ball A. (2006). SIMONE: Interplanetary Microsatellites for NEO Rendezvous Missions, *Acta Astronautica*, 59, 700-709.
2. Staab, D., et.al. (2018) XMET: A Xenon electrothermal thruster using additive manufacturing, *Space Propulsion Conference 2018 Seville*, 405.
3. Staab, D., et.al. (2019) XMET: Design and early Testing of a Xenon Microwave Electrothermal Thruster, *36th International Electric Propulsion Conference Vienna*, 405.
4. Hoffman, D. & Grubišić, A. (2019). Discharge-Mode Testing of the X-EPT Microwave ECR Gridded Ion Thruster. *36th Int. Electric Propulsion. Conf. Vienna*.
5. Reeve, S., et.al. (2020) Development Update of the X-EPT Microwave Gridded Ion Thruster for the IMPULSE Propulsion Architecture. *Space Propulsion Conference 2021*, 100.
6. Balaam, P. and Micci, M. M. (1995). Investigation of stabilized resonant cavity microwave plasmas for propulsion, *Journal of Propulsion Power*. 11:5, 1021-1027.
7. Gao, E. and Bilen, S.G. (2008). COMSOL Multiphysics Modeling of a 20W Microwave Electrothermal Thruster, *Proceedings of the 2008 COMSOL Conference*, Boston.
8. Clemens, D.E. (2008) Performance Evaluation of the Microwave Electrothermal Thruster Using Nitrogen, Simulated Hydrazine, and Ammonia. *PhD Dissertation, The Pennsylvania State University*.
9. Abaimov, M. D. (2015) Preliminary Testing of a 17.8-GHz Microwave Electrothermal Thruster for Small Spacecraft. *Master of Science Dissertation, The Pennsylvania State University*.
10. Werner, D. Momentus reports success in testing water plasma propulsion. *Space News [online]*, URL: <https://spacenews.com/momentus-el-camino-real-results/> [cited 25 Sept 2019].
11. Yildiz, M.S., Kokal, U. and Celik, M. (2017). Preliminary Thrust Measurement Results of the BUSTLab Microwave Electrothermal Thruster, *53rd Joint Propulsion Conference*, Atlanta, AIAA-2017-4725.
12. Romei, F., Grubisic, A., Gibbon, D., Lane, O., Hertford, R.A. and Roberts, G. (2015). A Thermo-fluidic Model for a Low Power Xenon Resistojet, *34th International Electric Propulsion Conference*, Kobe, IEPC-2015-265.